Electronic Supplementary Information

A Self-Reinforcing and Self-Healing Elastomer with High Strength, Unprecedented Toughness and Room-Temperature Reparability

Yuhan Li,[a] Wenjuan Li,[a] Ailing Sun,[a] Mengfan Jing,[c] Xingjiang Liu,[a] Liuhe Wei,*[a] Kai Wu,*[b] and Qiang Fu*[b]

[a] College of Chemistry and Green Catalysis Center, Zhengzhou Key Laboratory of Elastic Sealing Materials, Zhengzhou University, Zhengzhou 450001, China. E-mail: weiliuhe@zzu.edu.cn.
[b] College of Polymer Science and Engineering, State Key Laboratory of Polymer Materials and Engineering, Sichuan University. Chengdu 610065, China. E-mail: kaiwuscu@163.com; qiangfu@scu.edu.cn
[c] Key Laboratory of Materials Processing and Mold, National Engineering Research Center for Advanced Polymer Processing Technology, Zhengzhou University, Zhengzhou 450001, China.

Experimental Procedures

Materials

Polytetramethylene ether glycol (PTMEG, M_n = 1000 g/mol, f = 2), and dibutyltin dilaurate (DBTDL) were purchased from Aladdin. Isophorone diisocyanate (IPDI) was purchased from Adamas. 2, 6-Pyridinedimethanol (PDM), 1, 3-benzenedimethanol (BDM) and 2, 6-diaminopyridine (DAP) were purchased from Shanghai Bide Technology Co.,Ltd., and dried in a vacuum oven at 40 °C for 12 h before use. All of these chemical reagents were used without further purification. Toluene and tetrahydrofuran (THF) were purchased from Sinopharm Chemical Reagent Co., Ltd., and used after distillation.

Synthesis of polyurethane elastomers.

A series of PDM-based elastomers with various *R* values (defined as molar ratio of isocyanate groups to hydroxyl groups of PTMEG, [NCO]/[OH]) values were synthesized via identical process. In a typical process, PTMEG (20 g, 20.00 mmol) in a dried glass vessel equipped with a mechanical stirrer and a mercury thermometer was heated by an electric heating jacket at 120 °C under vacuum for 1 h to remove residual moisture and then cooled to 80 °C, IPDI (11.11 g, 50.00 mmol, *R* = 2.5) was added into the vessel and stirred for 1 h under argon atmosphere, then DBTDL (2.53 mg, 4.00×10^{-3} mmol) dissolved in anhydrous toluene was added into the vessel. The reaction was carried out at 80 °C for 3 h to obtain NCO-terminated polyurethane prepolymer mixing with marginal IPDI. Next, about 80 mL anhydrous toluene was added to adjust the viscosity, then PDM powder (4.17 g, 30.00 mmol) as the chain extender was directly added to the vessel. Note that protonic solvents like THF or DMF are not suitable in this system due to its presumable interference with carbamate formation caused by reducing reactivity of hydroxyl groups and interaction with pyridine ring. The reaction was continued until the NCO peak in the FTIR spectrum disappeared, during which it takes about 10 h. Finally, the viscous fluid was decanted into a rectangular mold and brought to vaporizing the solvent in a fume hood at ambient condition for 24 h and drying in oven at 80 °C for another 24 h, residual solvent was removed in a vacuum oven at 80 °C for 24 h, resulting in polyurethane elastomer film which is denoted as PDM-2.5. Other elastomers, PDM-2.1, PDM-2.3 and PDM-2.7, were synthesized with identical process except that the *R* values were adjusted to 2.1, 2.3 and 2.7, respectively. The BDM-2.5 elastomer was synthesized through an identical process except that the BDM was dissolved in anhydrous toluene before adding. The DAP-2.5 elastomer was also synthesized through an identical process to BDM-2.5 except that THF was adopted as the solvent.

Characterizations

The tensile tests were performed by stretching dumbbell samples (DIN 53504,Type S1) with a rate of 100 mm/min under ambient conditions (23 ± 2 °C, 50 ± 10% RH) on a tensile tester (TOPHUNG, TH-8203A, China) loaded with a 500 N load cell. For evaluation of SE, spliced samples were healed at 25 °C for a specific time before tensile tests. The SEs were calculated based on the recovery of tensile strength, elongation at break and toughness, which is expressed by the following eqation:

$$SE\ (\%) = (^{P_{healed}}/_{P_{original}} \times 100\ \%) \quad (1)$$

where P stands for tensile strength, elongation at break or toughness. For cyclic tests, the ultimate strain was set to 1000% and five consecutive cycles were conducted without intervals and the final cycle with 12 h interval at 25 °C. For facture tests, rectangular specimens with 50.0×5.0×1.0 mm dimension were stretched at a speed of 100 mm/min. The gauge length is 10.0 mm while the notch depth is 1.0 mm. Puncture tests were conducted on the same tensile tester equipped with a steel needle (Fig. S1) at a speed of 50

mm/min under compression mode. The puncture energy was calculated from the integrated area of the force-displacement curve. Stress relaxation experiments were carried out using a DMA Q800 (TA, USA) instrument. The strain amplitude was subjected to 100% at a specific temperature for 30 min. Rheological behaviors were measured with a rotating rheometer of TA instrument (DHR2, USA) using a 20 cm parallel plate-plate geometry. Frequency sweeping measurements were carried out with a strain amplitude of 0.1 % in the range of 0.1~100 Hz, and the temperature was accurately adjusted from 25 °C to 85 °C with a temperature interval of 10 °C. Master curves were constructed (25 °C as the reference) according to the principle of time-temperature superposition (TTS). The molecular weight information was obtained from gel permeation chromatography (GPC, Agilent LC2000, USA) at 25 °C equipped with a refractive index detector using THF as a mobile phase. Attenuated total reflectance FTIR spectra of bulk and reacting solutions were performed on a Bruker ALPHA II (Germany). Variable-temperature FTIR spectroscopy was performed on a Nicolet 6700 (Thermo Electron Corporation, USA). The temperature was set to rise from 25 °C to 105 °C with 5 °C interval. Variable-temperature ^{1}HNMR (DMF-d7) spectrum was recorded at 25 °C, 30 °C, 35 °C, 40 °C, 45 °C and 50 °C using a Bruker Avance 400 MHz (Germany) spectrometer. DSC measurements were carried out using a TA-DSC250 (USA) with a heating rate of 5 °C/min under nitrogen atmosphere. WAXS measurements were performed from a Nano-inXider SAXS/WAXS system (Xenocs, France, equipped with a microfocus sealed tube and an area detector, Cu Kα, λ = 1.54 Å). Samples were pre-stretched to a specific strain and then fixed before 120 s X-ray exposure. Observation of surface healing and SIC was conducted on a polarized optical microscopy (POM, Olympus BX61, Japan). Morphology of micro-phase separation was detected by AFM (TM-AFM, JPK Instruments, Germany). Transparency were measured by an UV-Vis spectrophotometer (Hewlett Packard 8453, G1103A, USA).

Quantum Chemistry Calculation

The hydrogen bond is expressed by the interaction energy (ΔE_H), which is the energy difference between the hydrogen bond complex (E_{AB}) and the monomers (E_A and E_B):

$$\Delta E_H = E_{AB} - E_A - E_B \quad (2)$$

The calculation uses ORCA software,[1] density functional theory, b3lyp method, def2-tzvp(-f) basis set to optimize the geometric structure and frequency calculation of the complex and the monomer, and obtain the electronic energy and zero-point energy correction. The model is visualized using VESTA.[2] The monomer structures A, B and C are illustrated in Fig. S2. And the energies are calculated as: (i) Total electronic energy E_A: -555.214 Hartree; (ii) Total electronic energy E_B: -323.336 Hartree; (iii) Total electronic energy E_C: -303.483 Hartree. The complex structures are shown in Fig. 3d, and the energies are calculated as follows: (i) Total electronic energy E_{AB}: -879.538 Hartree. Therefore the hydrogen bonding energy is: $\Delta E_H = E_{AB} - E_A - E_B$=-0.0122 Hartree = -7.686 kcal/mol, and the bonding energy of an individual A-B H-bond (pyridine-carbamate) is: 7.686 kcal/mol; (ii) Total electronic energy E_{BB}: -647.416 Hartree. Therefore, the hydrogen bond energy is: $\Delta E_H = E_{BB} - E_B - E_B$=-0.0116 Hartree = -7.326 kcal/mol, and the bonding energy of an individual B-B H-bond (carbamate-carbamate) is: 3.663 kcal/mol; (iii) Total electronic energy E_{CC}: -607.666 Hartree. Therefore the hydrogen bond energy is: $\Delta E_H = E_{CC} - E_C - E_C$=-0.0213 Hartree = -13.447 kcal/mol, and the bonding energy of an individual B-B H-bond (urea-urea) is: 13.447 kcal/mol.

Molecular Simulation method

Use molecular dynamics to calculate the interaction energy between molecular chains, in which PDM is 9 PDM-a units, 3 PDM-b units, and BDM is 9 BDM-a units, 3 BDM-b units, and DAP is 9 DAP-a units, 3 DAP-b units (Fig. S3a). All of the units are placed in a simulated box to represent the actual molecular chain configuration, and the initial configuration of the unit stacked in the box, use packmol set up.[3]

In the molecular dynamics calculations of the three molecular chains PDM, BDM, and DAP, the box size used in the simulation is 30Å × 30Å × 30Å, the force field used in the calculation is the cvff force field, and the atomic charge is the force field distribution. For each configuration, the energy is first performed minimize to convergence, and then perform molecular dynamics calculations, using NVT ensemble, simulation time 1000 ps, step length 1fs, temperature 298 K, until the system is balanced, and obtain non-bonded energy. The balanced structure is shown in the Fig. S3, and the visualization software is VMD.[4] The binding energy of PDM-9a/3b is 3778 kcal/mol, the binding energy of BDM-9a/3b is 3415 kcal/mol, and the binding energy of DAP-9a/3b is 5232 kcal/mol.

Results and Discussion

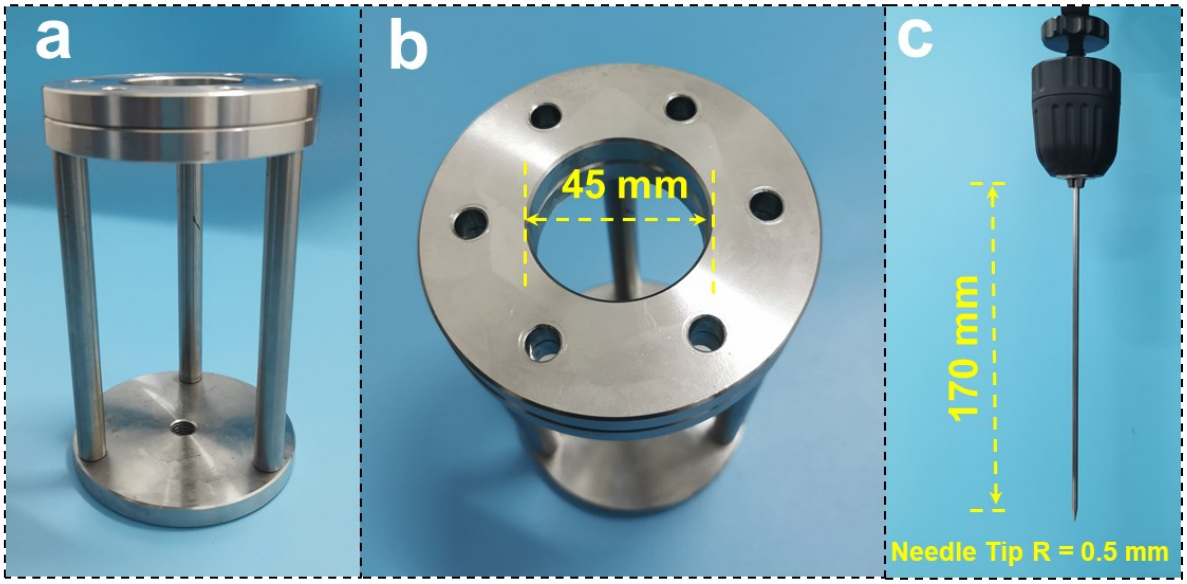

Fig. S1 Equipped tools for puncture tests of PDM-2.5 elastomer films: (a) and (b) Sapmple holder; (c) Steel needle (3.0 mm in diameter) fixed by a drill chuck.

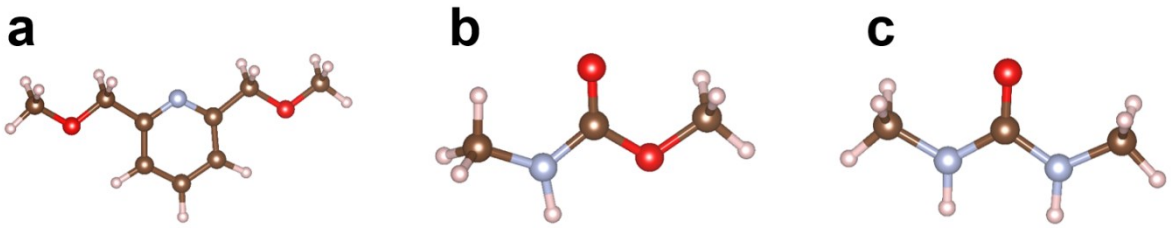

Fig. S2 Optimized molecular structures for simulation. (a) Monomer A, (b) Monomer B and (c) Monomer C.

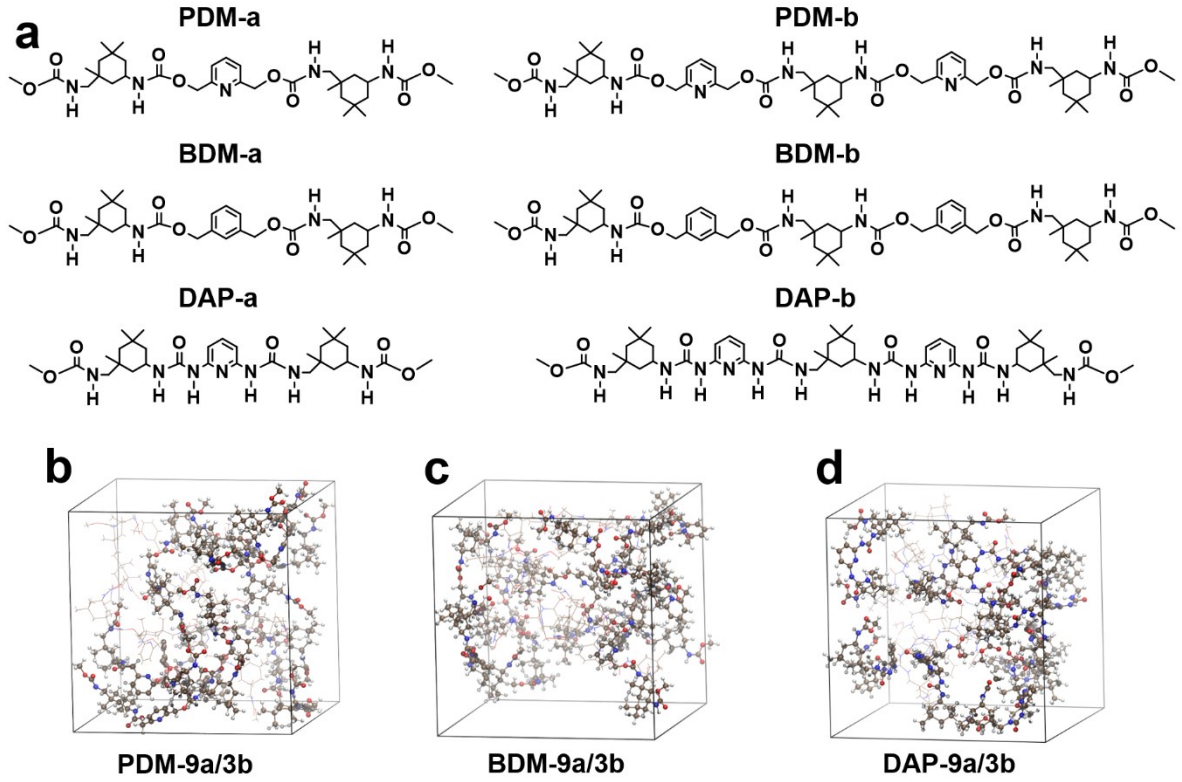

Fig. S3 Quantum chemical simulation of hard domains. (a) Optimized hard segments for simulations. Equilibrated configurations of (b) PDM-9a/3b, (c) BDM-9a/3b and (c) DAP-9a/3b.

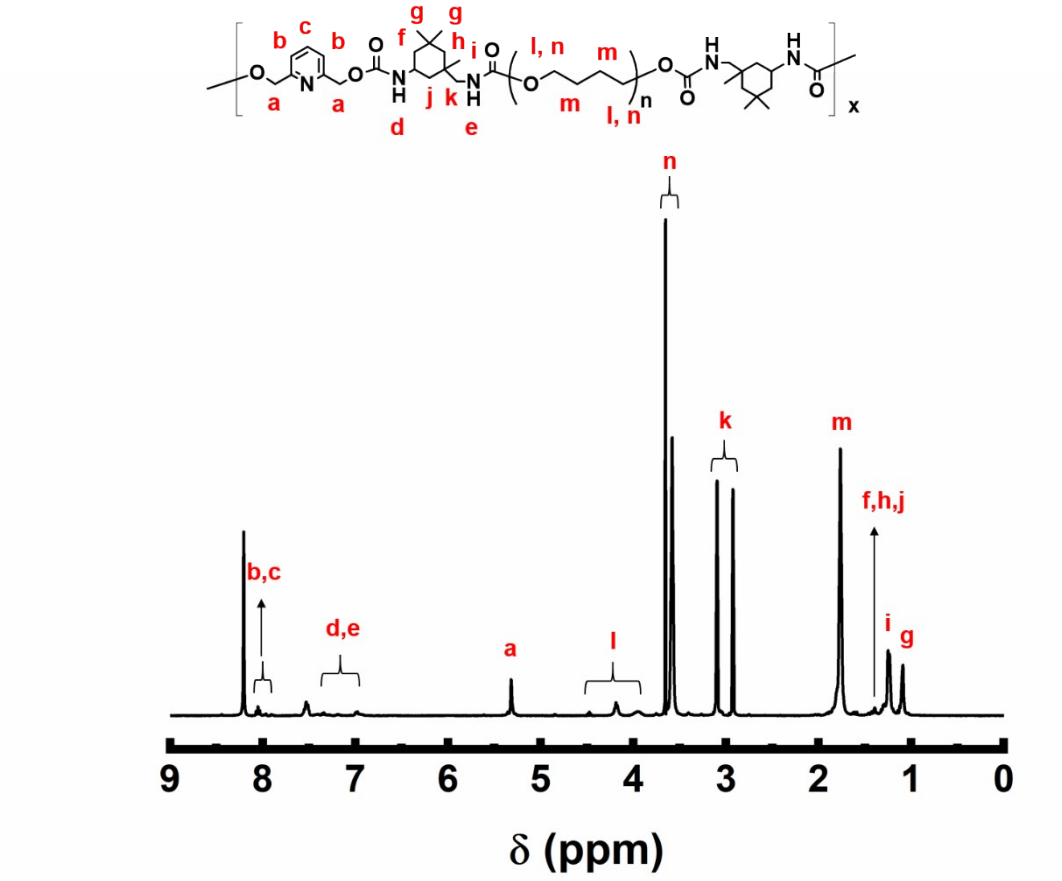

Fig. S4 ^{1}HNMR chemical shift of PDM-2.5.

The peak **l** assigns to hydrogen atoms in the repeating unit of PTMEG adjacent to the carbamate groups while the peak **n** assigns to identical-sited hydrogen atoms which are not adjacent to the carbamate groups.

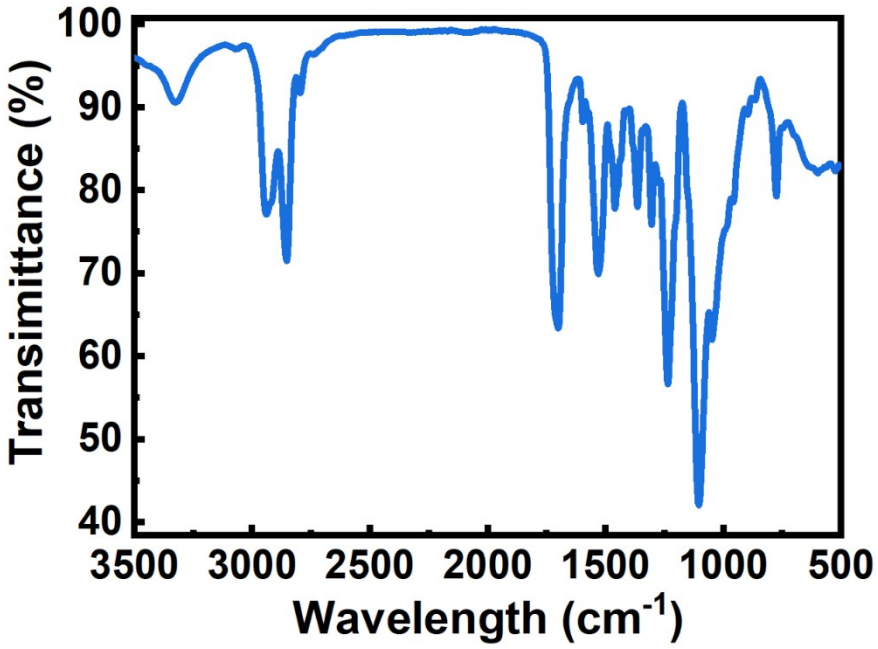

Fig. S5 FTIR spectrum of PDM-2.5.

Detailed peak assignments are listed in Table S1.

Table S1 Characteristic peak assignments of PDM-2.5.

Assignments	PDM-2.5
	Wavenumber (cm^{-1})
free ν (N-H)	3454
H-bonded ν (N-H)	3327
ν_a (CH_2)	2943
ν_a (CH_2)	2918
ν_s (CH_2)	2856
ν_s (CH_2)	2797
free ν (C=O) amide I	1715
H-bonded ν (C=O) amide I	1701
ν (pyridine ring)	1598, 1576
H-bonded ν (C-N) + δ (N-H) amide II	1538
free ν (C-N) + δ (N-H) amide II	1532
H-bonded ν (C-N) + δ (N-H) amide III	1237
free ν (C-N) + δ (N-H) amide III	1218
ν (C-O-C)	1106

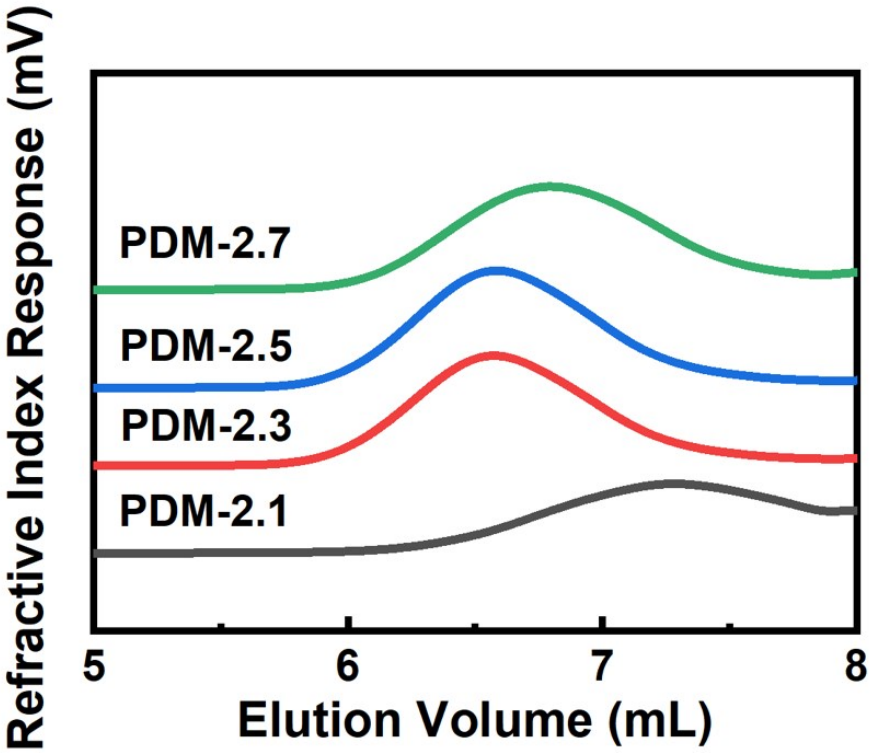

Fig. S6 THF-GPC profiles of polyurethane extended by PDM.

Table S2 Molecular weight information of polyurethane extended by PDM.

Sample	M_n (g/mol)	M_w (g/mol)	PDI[a]
PDM-2.1	4.2078×10^4	7.9663×10^4	1.89
PDM-2.3	6.2871×10^4	1.1777×10^5	1.87
PDM-2.5	6.1078×10^4	1.1490×10^5	1.88
PDM-2.7	4.4548×10^4	8.2655×10^4	1.86

[a] polydispersity index.

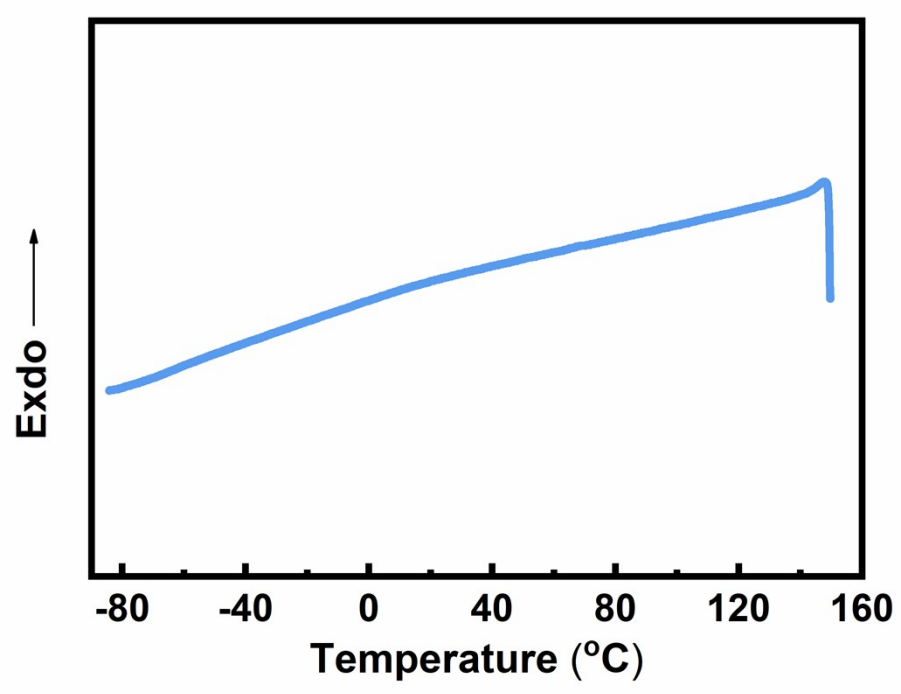

Fig. S7 DSC curves of PDM-2.5 with temperature decreasing.

DSC curves of the as-synthesized elastomer PDM-2.5 have no distinct peak of glass transition temperature (T_g) in the range from -85 °C to 150 °C but two obvious gentle slope in a wide range. This is probably related to the loosely-packed aggregation of hard segments and the randomly arranged soft segments due to its low content.

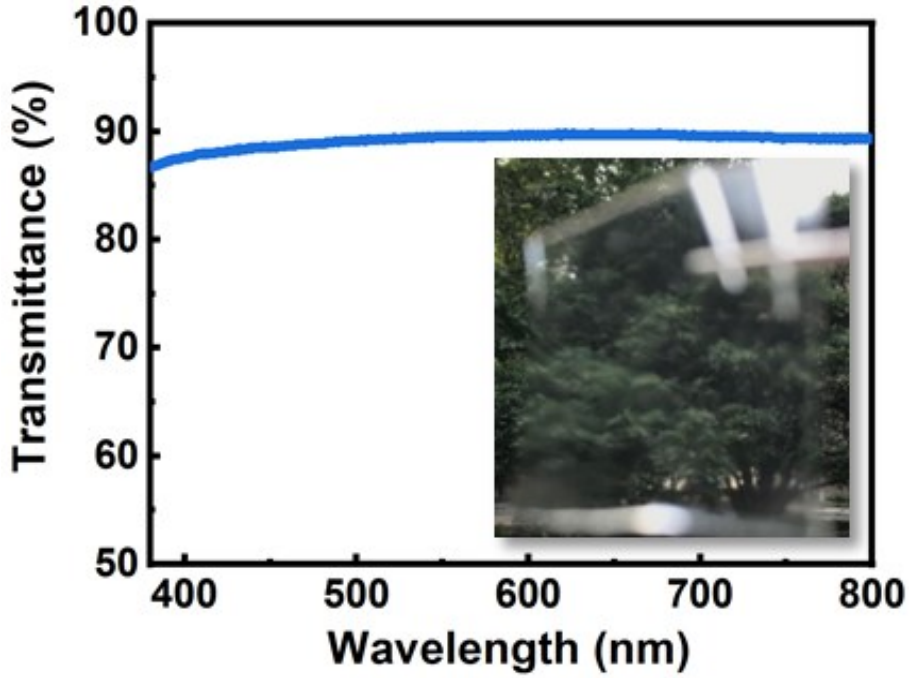

Fig. S8 Transparency of PDM-2.5 elastomer.

Film thickness is ~0.5 mm, and the transmittance at 600 nm is ~90%.

Table S3 Comparison of mechanical properties of PDM-2.5 elastomer with synthetic room-temperature self-healable materials in the previous literatures.

Sample Name	Strength (MPa)	Elongation (%)	Toughness (MJ/m^3)	Fracture energy (kJ/m^2)	Ref.
PDM-2.5	29.0 ± 0.9	1806 ± 39	121.8 ± 8.5	104.1	This work
PSeD-U20-12h	2.42	509	4.59	3.67	5
PPGTD-IDA	4.83	2010	65.49	42.65	6
PEG-DE-CAT-DAB	21.9	≈170	22	/	7
ICPs-Zn$(NTf_2)_2$	≈1.25	≈470	~9.8	/	8
IP-SS	6.76	923	26.9	/	9
Cu-DOU-CPU	14.8	1182	87	/	10
DOU-CPU	6.8	901	39	/	10
PI-58NA	7	13400	70	/	11
P-Cur-Eu	1.8	886	/	2.44	12
$EA_{0.5}$	16	≈225	/	5	13
Fe-Hpdca-PDMS	≈0.25	2000	/	2.57	14
AA-DADD-HMDA	≈20	≈170	/	13.5	15
C_{mon}	≈0.5	≈4500	/	2.1	16
U-PDMS	1.11	984	7.14	/	17
PEIs	4.4	560	12	/	18
PDMS	0.23	1850	3.8	/	14
P(DA-*co*-BA)	3.5	310	6.8	/	19
PDMS-PtL	0.3	1400	3.4	/	20
Poly(urea-urethane)	0.81	3100	13	/	21
HBPs	1.9	780	10	/	22
CB[8] polymer	0.5	≈4500	≈11	/	16
SPM-2	≈0.8	17000	/	30	23

Table S4 Mechanical properties of polyurethane elastomers with various *R* values extended by PDM.

Sample Name	Strength (MPa)	Elongation (%)	Toughness (MJ/m^3)
PDM-2.1	0.8 ± 0.1	2603 ± 58	10.2 ± 0.6
PDM-2.3	7.3 ± 0.4	1902 ± 38	52.8 ± 4.0
PDM-2.5	29.0 ± 0.9	1806 ± 39	121.8 ± 8.5
PDM-2.7	33.7 ± 0.9	1745 ± 38	147.2 ± 3.0

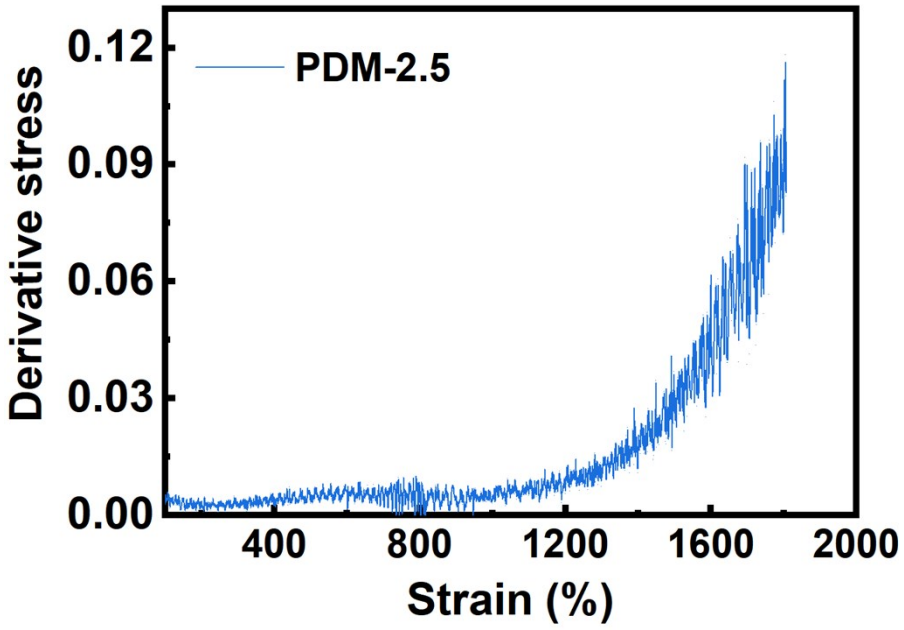

Fig. S9 Derivative stress versus strain curve of PDM-2.5 for illustrating the changing rate of tensile strength.

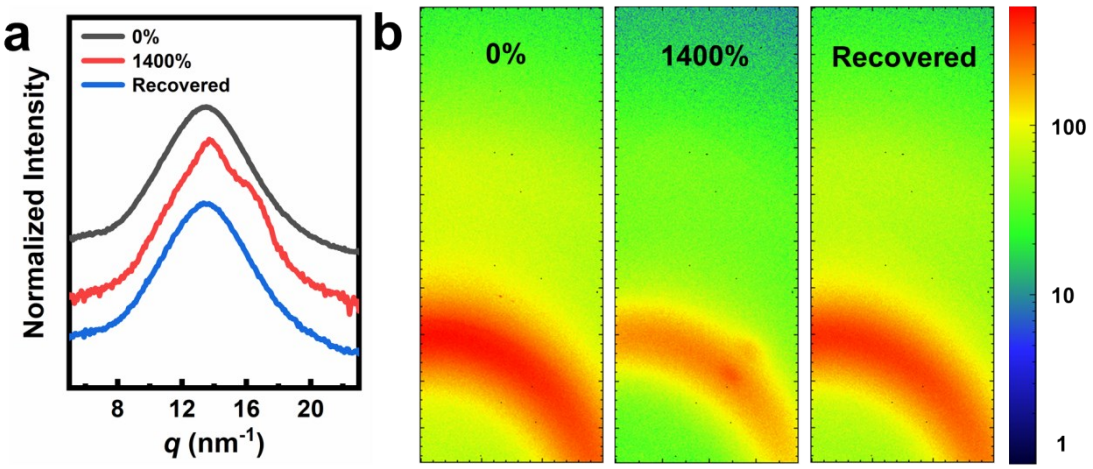

Fig. S10 (a) 1D WAXS results of PDM-2.5 stretched to 1400% and subsequently recovered for 1 h at room temperature; (b) Corresponding 2D WAXS patterns.

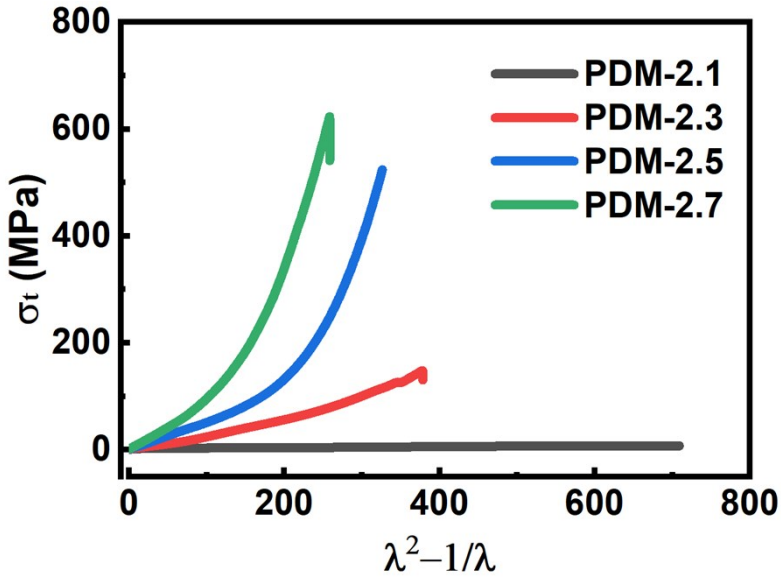

Fig. S11 True stress σ_t versus (λ^2-1/λ) curves of various elastomers.

The true stress σ_t and elongation ratio λ are deduced from the engineering stress (σ_e) and strain (ε_e), which are both directly recorded by the tensile tester. Specifically, $\varepsilon_e = l / l_0 - 1 = \lambda - 1$, where l and l_0 represents the length of sample after drawn and gauge length, respectively. The σ_t is defined as F/A, where F and A are the loading force and actual cross-sectional area which could be express as $A = A_0 / (1+ \varepsilon_e)$. A_0 stands for the initial cross-sectional area before stretching. Thus, the σ_t could be converted to $\sigma_t = \sigma_e / (1+ \varepsilon_e)$. The curves of σ_t plotted to (λ^2-1/λ) could be fitted with a function of $\sigma_t = Y + G_p (\lambda^2\text{-}1/\lambda)$, where Y relates to the extrapolated yield stress and G_p (MPa) is defined as the strain hardening modulus. G_p could be further express as a function of $\rho RT/ \bar{M}_c$, where ρ (g/cm^3) is the density of materials, R (J/(mol·K)) is the ideal gas constant, T (K) is the absolute temperature and $\bar{M}_c$ (g/mol) is the average constraint molecular weight between the physical crosslinking junctions, hereby hard domains of aggregated hard segments. As the material density ρ is measured to be ~1.068 g/cm^3, $\bar{M}_c$ of PDM-2.1, PDM-2.3, PDM-2.5, PDM-2.7 is calculated to be 9980, 6503, 5518 and 3372 g/mol, respectively.

It is found that each $\bar{M}_c$ is not necessarily approximate to the molecular weight of PTMEG soft segment (1000 g/mol), instead that it is a certain times of PTMEG chains. Accordingly, it can be assumed that there exist hard segments that do not participate in microphase separation. These hard segments together with their adjacently-connected soft segments are regarded as effective soft chains. Based on this, low $\bar{M}_c$ means less PTMEG chain blocks between crosslinking junctions are available for SIC. In the meantime, these blocks are less entangled which is favorable for SIC whereas the short distance between crosslinking junctions in this case would restrict the regularity of oriented arrangement of these block during stretching. Thus, regulating SIC needs a balance among these mutually exclusive factors. The stress-strain curve of PDM-2.5 indicates that it has an ideal $\bar{M}_c$, i.e. suitable effective length of crystaliizable segments, to generate the most obvious phenomenon of SIC.

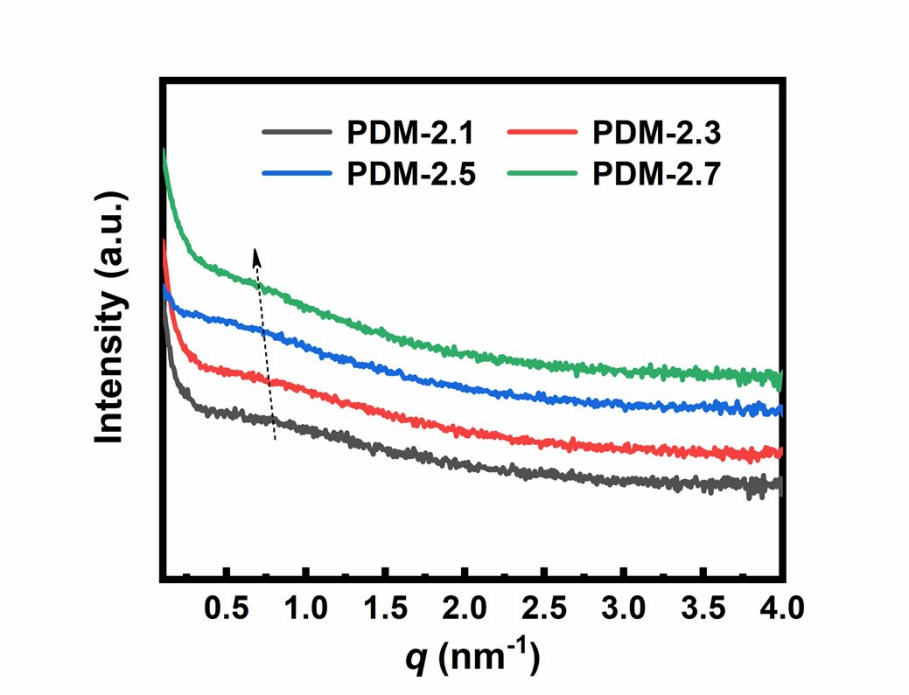

Fig. S12 SAXS results of PDM-based elastomers without stretching.

A bump peak can be observed for each sample. The relative *q* vector tends to undergo downshift as the *R* value increases. It signifies that the average size of hard domains (idealized as spherical model) gradually increases with the increase of hard phase content, validating the feasibility of regulating hard phase through adjusting *R* value. The flattened peak indicates that the hard domains are loosely-packed. In addition, the downshift of peak *q* vector also confirms that the chain length constraint between physical crosslinking junctions is shortened.

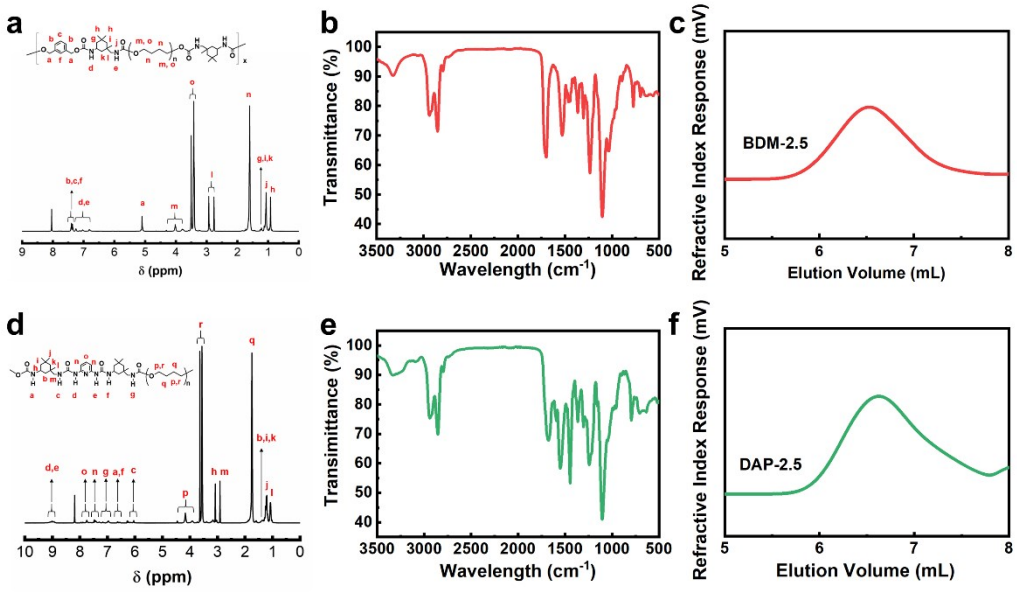

Fig. S13 Characterizations of elastomers. (a) ^{1}HNMR chemical shift, (b) FTIR spectrum and (c) THF-GPC profile of BDM-2.5; (d) ^{1}HNMR chemical shift, (e) FTIR spectrum and (f) THF-GPC profile of DAP-2.5.

For ^{1}HNMR of BDM-2.5, the peak **m** assigns to hydrogen atoms in the repeating unit of PTMEG adjacent to the carbamate group while the peak **o** assigns to identical-sited hydrogen atoms which are not adjacent to the carbamate group. The same situation at peak **p** and peak **r** for DAP-2.5.

Table S5 Molecular weight information of BDM-2.5 and DAP-2.5.

Sample	M_n (g/mol)	M_w (g/mol)	PDI
BDM-2.5	6.9958×10^4	1.4087×10^5	2.01
DAP-2.5	3.8092×10^4	7.3116×10^4	1.92

Table S6 Characteristic peak assignments of BDM-2.5.

Assignment	BMD-2.5
	Wavenumber (cm^{-1})
free ν (N-H)	3452
H-bonded ν (N-H)	3327
ν_a (CH_2)	2942
ν_a (CH_2)	2917
ν_s (CH_2)	2856
ν_s (CH_2)	2796
free ν (C=O) amide I	1716
H-bonded ν (C=O) amide I	1700
ν (aromatic ring)	1616, 1594
H-bonded ν (C-N) + δ (N-H) amide II	1539
free ν (C-N) + δ (N-H) amide II	1531
H-bonded ν (C-N) + δ (N-H) amide III	1236
Free ν (C-N) + δ (N-H) amide III	1219
ν (C-O-C)	1106

Table S7 Characteristic peak assignments of DAP-2.5.

Assignment	DAP-2.5
	Wavenumber (cm^{-1})
free ν (N-H)	3489
H-bonded ν (N-H)	3346,3238
ν_a (CH_2)	2942
ν_a (CH_2)	2916
ν_s (CH_2)	2858
ν_s (CH_2)	2797
free ν (C=O) amide I	1678
H-bonded ν (C=O) amide I	1701
Disordered H-bonded ν (C=O) amide I	1656
Ordered H-bonded ν (C=O) amide I	1626
H-bonded ν (pyridine ring)	1604
Free ν (pyridine ring)	1598
H-bonded ν (C-N) + δ (N-H) amide II	1562,1558
free ν (C-N) + δ (N-H) amide II	1552
H-bonded ν (C-N) + δ (N-H) amide III	1243
free ν (C-N) + δ (N-H) amide III	1219
ν (C-O-C)	1101

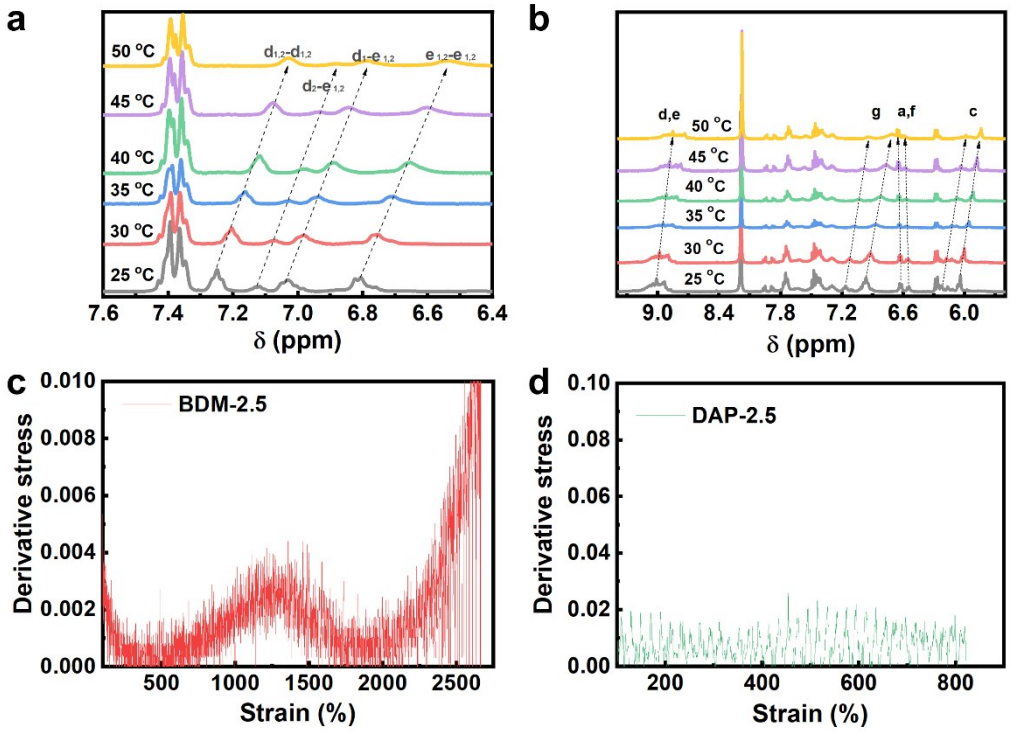

Fig. S14 Evolution of characteristic peaks in variable-temperature ^{1}HNMR related to H-bonding interactions at various temperatures. (a) BDM-2.5 and (b) DAP-2.5; Derivative stress against strain curves of (c) BDM-2.5 and (d) DAP-2.5.

The peak **d** and **e** of BMD-2.5 (refer to Fig. S13a) could be further split into $\mathbf{d_1}$, $\mathbf{d_2}$, $\mathbf{e_1}$ and $\mathbf{e_2}$ due to distinct connection between BDM and the two active sites of IPDI. Detailed configurations of H-bonding pairs are shown in Fig. S19.

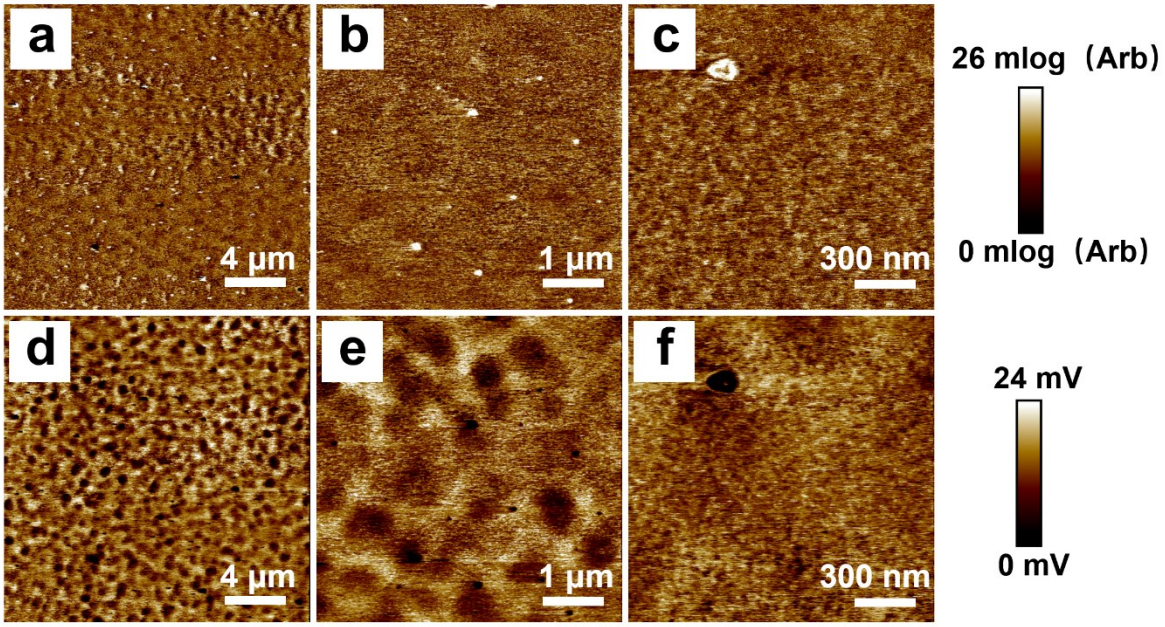

Fig. S15 AFM images of PDM-2.5. (a), (b) and (c) are the modulus images; (d), (e) and (f) are the adhesion images.

The hard segments are relatively higher in rigidity and polarity, so the modulus and adhesion signal probed by AFM is displayed in brighter color, which serves to reflect the morphology of the phase seperation of PDM-2.5. Both of modulus and adhesion images demonstrates that the hard segemnts assemble into nano-scale, loosely-packed domains because the bondary is indistinct and the shape is irregualar to recognize.

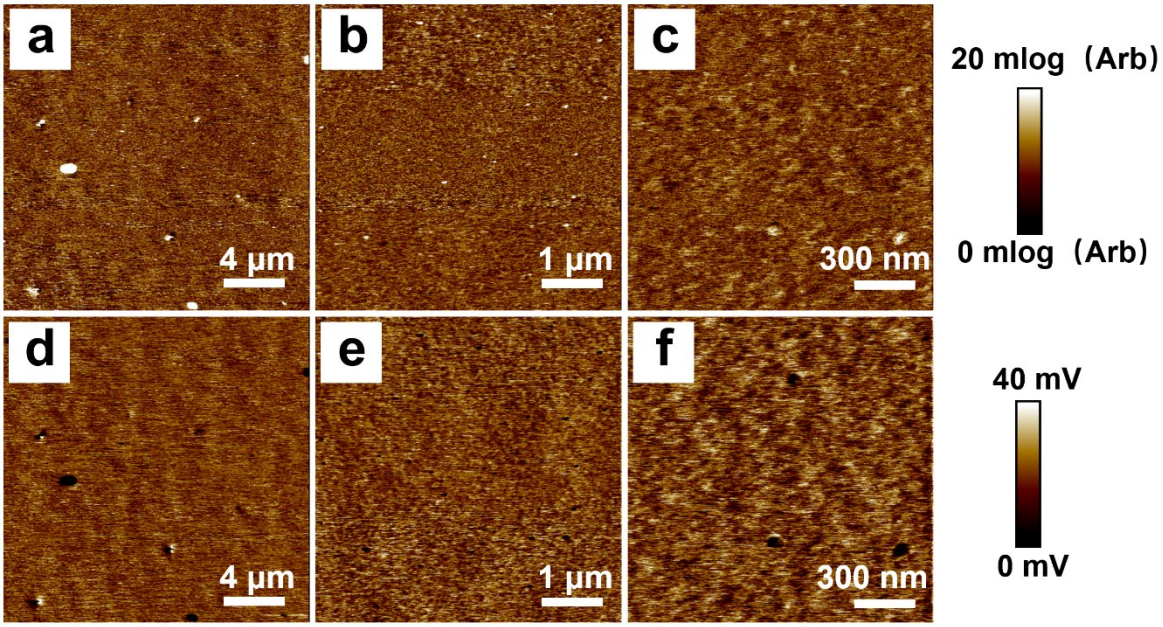

Fig.S16 AFM images of BDM-2.5. (a), (b) and (c) are the modulus images; (d), (e) and (f) are the adhesion images.

The morphology of the phase seperation of BDM-2.5 is similar to that of PDM-2.5, i.e. hard segemnts assemble into nano-scale, loosely-packed domains because the bondary is indistinct and the shape is irregualar to recognize.

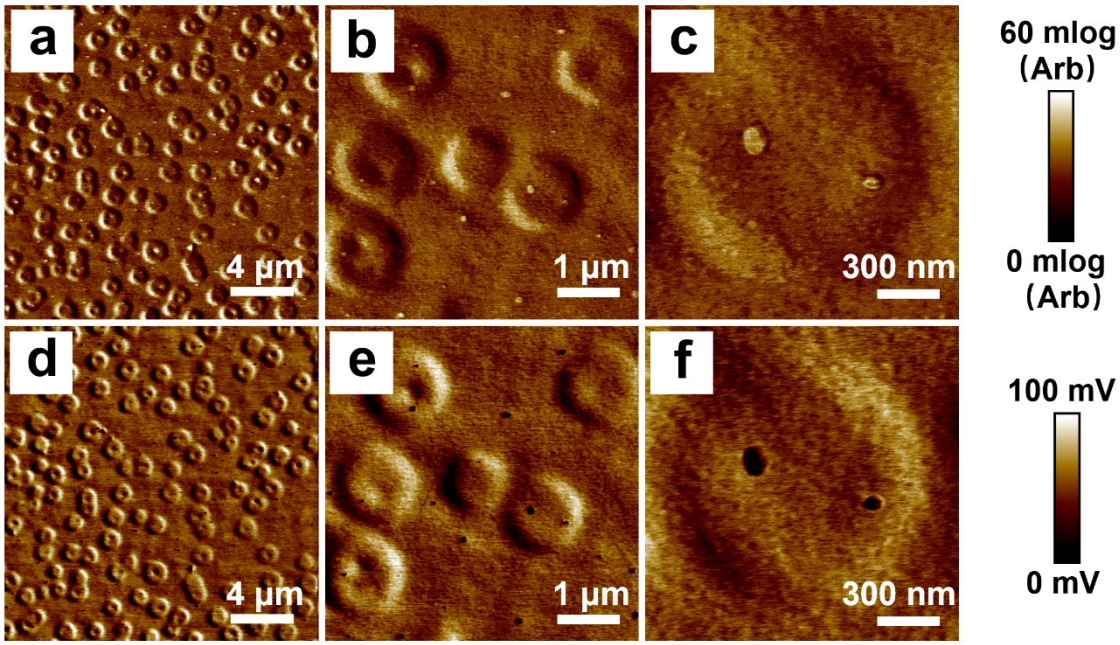

Fig. S17 AFM images of DAP-2.5. (a), (b) and (c) are the modulus images; (d), (e) and (f) are the adhesion images.

The morphology of the phase seperation of DAP-2.5 is different from that PDM-2.5 and BDM-2.5. The hard segemnts is likely to intimately assemble into dense and compact domains although no regular hard domains are also not observed.

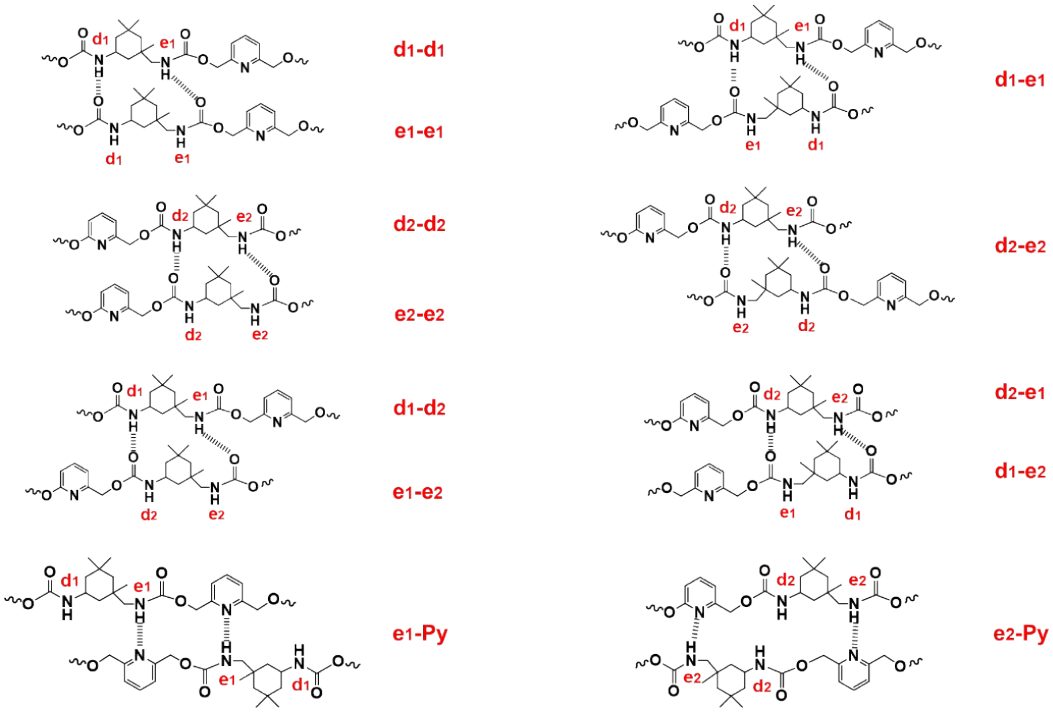

Fig. S18 Configurations of H-bonding pairs for PDM-2.5 elastomer.

The peak **d** and **e** (refer to Fig. S4) could be further splited into $\mathbf{d_1}$, $\mathbf{d_2}$, $\mathbf{e_1}$ and $\mathbf{e_2}$ due to distinct connection between PDM and the two active sites of IPDI. The evolution of chemical shift is listed in Table S8.

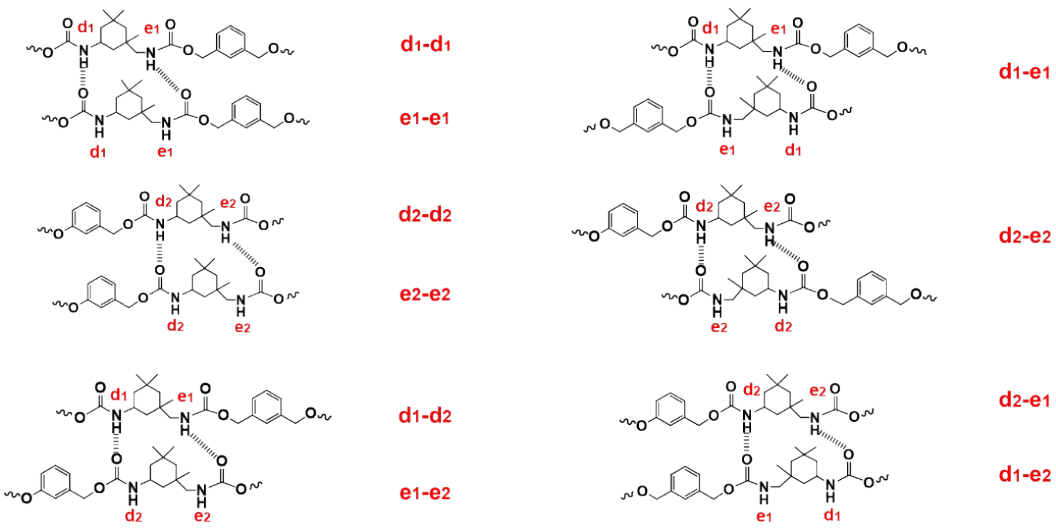

Fig. S19 Configurations of H-bonding pairs for BDM-2.5 elastomer.

The peak **d** and **e** (refer to Fig. S13a) could be further splited into $\mathbf{d_1}$, $\mathbf{d_2}$, $\mathbf{e_1}$ and $\mathbf{e_2}$ due to distinct connection between BDM and the two active sites of IPDI. The evolution of chemical shift is listed in Table S8.

Table S8 Detailed H-bonding pairs and evolution of corresponding chemical shift of PDM-2.5 and BDM-2.5 elastomers at different temperatures.

Sample	Temperature (°C)	carbamate-carbamate				pyridine-carbamate
		$d_{1,2}$-$d_{1,2}$	d_1-$e_{1,2}$	d_2-$e_{1,2}$	$e_{1,2}$-$e_{1,2}$	$e_{1,2}$-Py
BDM-2.5	25	7.23/7.25/7.26	7.03/7.05	7.12/7.13	6.81/6.82	N.E.[a]
	30	7.19/7.20/7.22	6.98/7.00	7.07/7.08	6.75/6.77	N.E.
	35	-/7.16/-	6.94/-	7.03/7.04	6.71/6.72	N.E.
	40	-/7.12/-	6.89/-	6.98/-	6.65/6.66	N.E.
	45	-/7.08/-	6.84/-	6.93/-	6.60/-	N.E.
	50	-/7.03/-	6.79/-	6.87/-	6.54/-	N.E.
PDM-2.5	25	7.55/-/-/-[b]	7.34/7.36	7.40/7.42	6.98/7.00	7.18/7.20
	30	-/-/7.48/7.50[c]	7.30/7.32	7.36/7.38	6.93/6.95	7.14/7.16
	35	7.44/7.46/7.47/7.44	7.25/7.27	7.31/7.33	6.89/6.91	7.09/7.11
	40	7.40/7.41/7.43/7.44	7.20/7.22	7.27/-	6.84/-	7.05/7.07
	45	7.35/7.37/7.38/7.40	7.16/7.18	7.23/-	6.79/-	7.02/-
	50	-/7.33/7.34/-	7.11/-	7.18/-	6.73/-	6.97/-

[a]: not existing; [b]: three peaks covered by pyridinal hydrogen peaks; [c]: two peaks covered by pyridinal hydrogen peaks. All of the characteristic peaks could be categorized into peak groups according to the specific chemical shift. PDM-2.5 has five peak groups undergoing upfield shift as the temperature increases while BMD-2.5 has four peak groups undergoing upfield shift.

Table S9 Comparison of the mechanical properties of the three elastomers.

Sample Name	Strength (MPa)	Elongation (%)	Toughness (MJ/m^3)
PDM-2.5	29.0 ± 0.9	1806 ± 39	121.8 ± 8.5
BDM-2.5	6.0 ± 1.3	2655 ± 13	61.0 ± 7.4
DAP-2.5	3.6 ± 0.4	1055 ± 44	30.8 ± 3.1

Table S10 Mechanical properties and SEs of PDM-2.5 healed for different hours.

Time (h)	Tensile strength (MPa)	Elongation (%)	Toughness (MJ/m³)	Tensile $strength_{SE}$ (%)	$Elongation_{SE}$ (%)	$Toughness_{SE}$ (%)
Raw	29.0 ± 0.9	1806 ± 39	121.8 ± 8.5	/	/	/
3	3.6 ± 0.4	694 ± 103	15 ± 3.3	12.4 ± 1.5	38.4 ± 5.7	12.3 ± 2.7
6	3.8 ± 0.8	1143 ± 265	24.5 ± 9.5	8.6 ± 2.7	42.2 ± 14.7	13.4 ± 7.8
9	5.8 ± 0.5	1440 ± 156	42.1 ± 7.0	19.9 ± 1.6	79.7 ± 8.6	34.6 ± 5.7
12	20.7 ± 2.8	1757 ± 35	94.0 ± 7.4	71.4 ± 9.8	97.3 ± 1.9	77.1 ± 6.1
24	25.8 ± 4.8	1804 ± 64	111.7 ± 13.6	81.3 ± 16.5	98.6 ± 3.6	86.5 ± 11.2

Table S11 SEs of PDM-based elastomers healed for 12 h.

Sample	Tensile strength$_{SE}$ (%)	Elongation$_{SE}$ (%)	Toughness$_{SE}$ (%)
PDM-2.1	100.2 ± 1.8	99.0 ± 0.9	102.9 ± 5.5
PDM-2.3	92.2 ± 5.5	98.7 ± 2.5	96.7 ± 2.6
PDM-2.5	71.4 ± 9.8	97.3 ± 1.9	77.1 ± 6.1
PDM-2.7	33.5 ± 0.8	76.6 ± 3.9	40.9 ± 2

Table S12 SEs of PDM-based elastomers healed for 24 h.

Sample	Tensile strength$_{SE}$ (%)	Elongation$_{SE}$ (%)	Toughness$_{SE}$ (%)
PDM-2.1	99.4 ± 2.7	98.8 ± 3.6	104.4 ± 3.5
PDM-2.3	93.0 ± 6.6	99.4 ± 4.5	102.5 ± 10.5
PDM-2.5	81.3 ± 16.5	98.6 ± 3.6	86.5 ± 11.2
PDM-2.7	39.0 ± 2.7	82.6 ± 2.8	49.5 ± 1.2

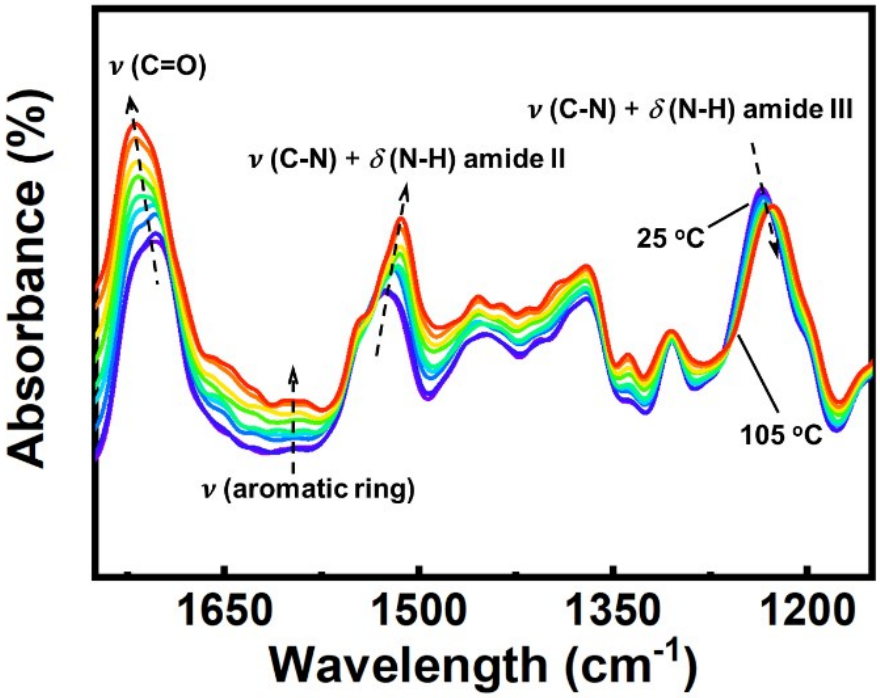

Fig. S20 Variable-temperature FTIR spectra of BDM-2.5 with temperature varying from 25 °C to 105 °C.

Characteristic peaks of ν (C=O), amide II and amide III occur shift which is actually simultaneous attenuation of free peaks and decline of H-bonded peakes. While for PDM-2.5, an additional peak related to ν (pyridine ring) also occurs slight shift (Fig. 4d), which confirms the existence of pyridine-carbamate H-bonding and its room-temperature reversibility.

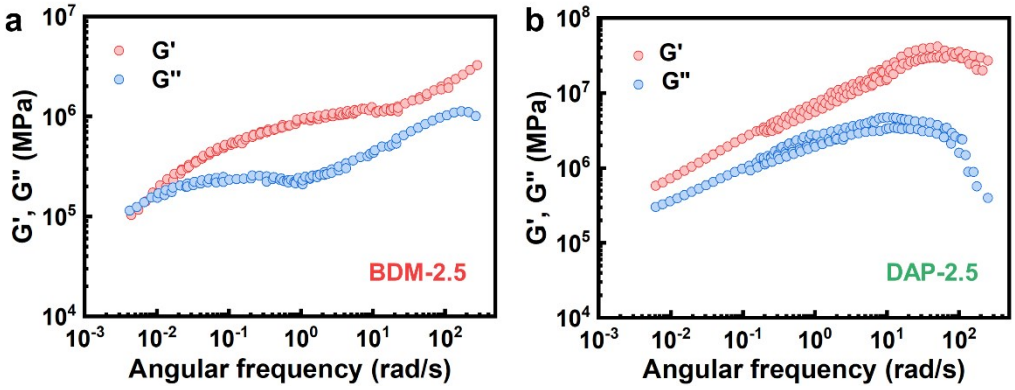

Fig. S21 Rheological master curves of (a) BDM-2.5 and (b) DAP-2.5 elastomers.

The crossover point (ω_c) at G′ = G″ in the master curves is a symbolic transition of elastomer network from physically crosslinked and elastic state to reversible and fluid-like state. The reciprocal of τ_c relates to the characteristic relaxation time (τ_c) that reflects the time it takes to perform such transition, and it can be also understood as a factor reflecting the chain mobility. The ω_c of PDM-2.5 (Fig. 4e) and BDM-2.5 is 6.797×10^{-2} rad/s and 0.775×10^{-2} rad/s, respectively. Thus, the corresponding τ_c is calculated to be 924.9 s and 810.3 s, respectively. There is no crossover point for DAP-2.5.

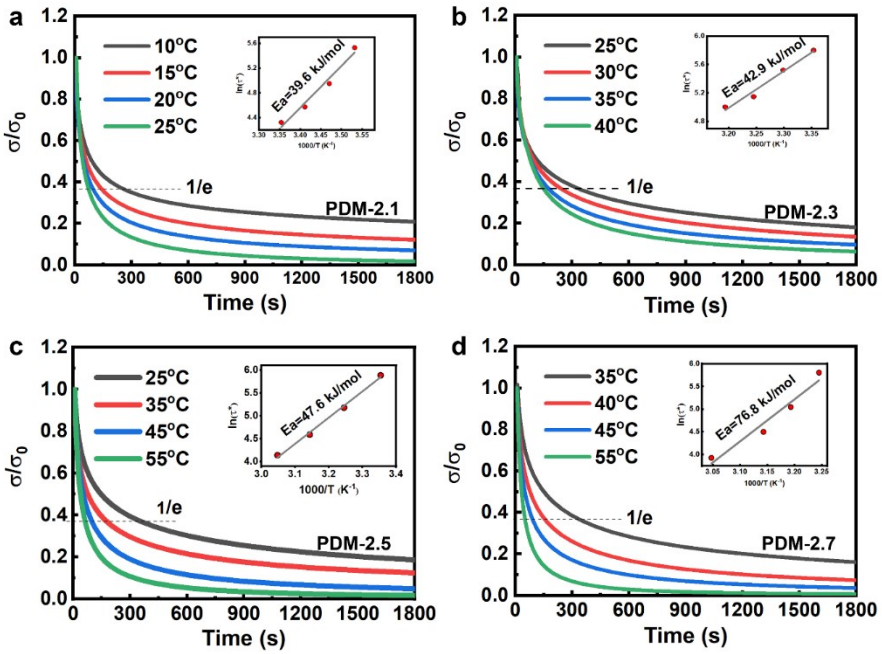

Fig. S22 Stress relaxation results of (a) PDM-2.1, (b) PDM-2.3, (c) PDM-2.5 and PDM-2.7 elastomers.

The activation energy (E_a) is calculated by Arrhenius equation:

$$\tau(T) = \tau_0 exp(E_a/RT) \quad (3)$$

where $\tau(T)$ is the stress relaxation time at temperature T (K), τ_0 is a constant, E_a is the relaxation activation energy and R is the ideal gas constant. $\tau(T)$ can be directly deduced from the following equation with reference to relaxation curves:

$$\sigma = \sigma_0 \, exp(-t/\tau) \quad (4)$$

where σ_0 (MPa) is the initial stress, σ is the stress at time t (s), and the relaxation time τ_c is determined as the time when σ_0 = 1/e. The stress relaxation time τ_c of PDM-2.5 at 25 °C is ~360 s, which indicates fast rearrangement of hard segments through dissociation-association of hierarchical H-bonds. The discrepancy of E_a is basically originated from content of hard segments, i.e. the amount of hierarchical H-bonds.

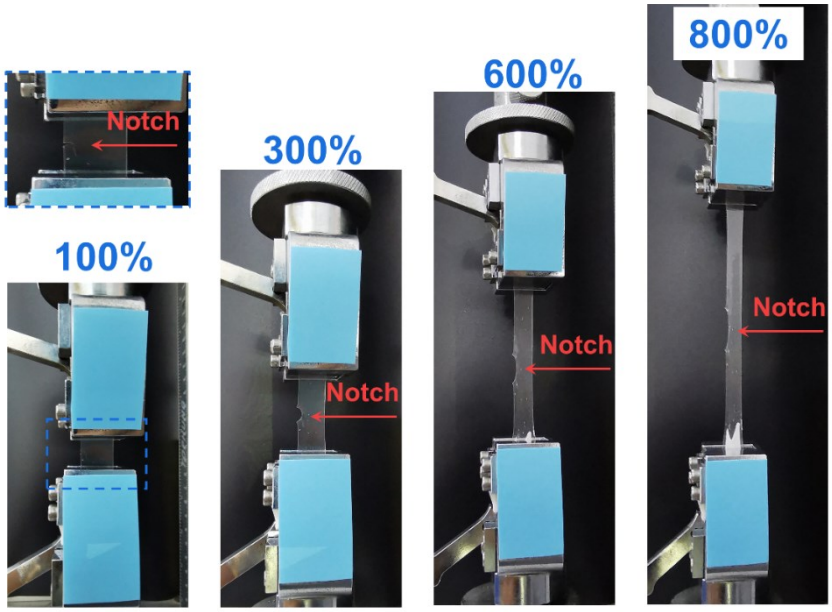

Fig. S23 Observation of the process of the fracture energy tests.

References

1 F. Neese, *The ORCA program system,* 2012, **2**, 6.
2 K. Momma, Izumi,F., *J. Appl. Crystallogr.,* 2011, **44**, 5.
3 L. Martínez, R. Andrade, E. G. Birgin, J. M. Martínez, *J.Comput. Chem.,* 2009, **30**, 2157-2164.
4 W. Humphrey, A. Dalke, K. Schulten, *J.Mol. Graph.,* 1996, **14**, 33-38.
5 S. Chen, L. Sun, X. Zhou, Y. Guo, J. Song, S. Qian, Z. Liu, Q. Guan, E. Meade Jeffries, W. Liu, Y. Wang, C. He, Z. You, *Nat. Commun.,* 2020, **11**, 1107.
6 D. Wang, J. Xu, J. Chen, P. Hu, Y. Wang, W. Jiang, J. Fu, *Adv. Funct. Mater.,* 2019, 1907109-1907122.
7 E. Filippidi, T. R. Cristiani, C. D. Eisenbach, J. H. Waite, J. N. Israelachvili, B. K. Ahn, M. T. Valentine, *Science,* 2017, **358**, 502-505.
8 D. Mozhdehi, S. Ayala, O. R. Cromwell, Z. Guan, *J. Am. Chem. Soc.,* 2014, **136**, 16128-16131.
9 S. Kim, H. Jeon, S. Shin, S. Park, J. Jegal, S. Y. Hwang, D. X. Oh, J. Park, *Adv. Mater.,* 2018, **30**, 1705145-1705152.
10 L. Zhang, Z. Liu, X. Wu, Q. Guan, S. Chen, L. Sun, Y. Guo, S. Wang, J. Song, E. M. Jeffries, C. He, F.-L. Qing, X. Bao, Z. You, *Adv. Mater.,* 2019, 1901402-1901509.
11 Y. Miwa, J. Kurachi, Y. Kohbara, S. Kutsumizu, *Commun. Chem.,* 2018, **1**, 5.
12 Q. Zhang, S. Niu, L. Wang, J. Lopez, S. Chen, Y. Cai, R. Du, Y. Liu, J. Lai, L. Liu, C. Li, X. Yan, C. Liu, J. B.-H. Tok, X. Jia, Z. Bao, *Adv. Mater.,* 2018, **30**, 1801435.
13 E. Ducrot, Y. Chen, M. Bulters, R. P. Sijbesma, C. Creton, *Science,* 2014, **344**, 186-189.
14 C. Li, C. Wang, C. Keplinger, J.-L. Zuo, L. Jin, Y. Sun, P. Zheng, Y. Cao, F. Lissel, C. Linder, X. You, Z. Bao, *Nat. Chem.* 2016, *8*, 618-624.
15 J. Wu, L. Cai, D. A. Weitz, *Adv. Mater.,* 2017, **29**, 1702616.
16 J. Liu, C. S. Y. Tan, Z. Yu, N. Li, C. Abell, O. A. Scherman, *Adv. Mater.,* 2017, **29**, 1605325.
17 P.Cao, B. Li, T. Hong, J. Townsend, Z. Qiang, K. Xing, K. D. Vogiatzis, Y. Wang, J. W. Mays, A. P. Sokolov, T. Saito, *Adv. Funct. Mater.,* 2018, **28**, 1800741.
18 A. Susa, R. K. Bose, A. M. Grande, S. van der Zwaag, S. J. Garcia, *ACS Appl. Mater. Inter.,* 2016, **8**, 34068-34079.
19 J. Li, H. Ejima, N. Yoshie, *ACS Appl. Mater. Inter.,* 2016, **8**, 19047-19053.
20 J. Mei, X. Jia, J. Lai, Y. Sun, C. Li, J. Wu, Y. Cao, X. You, Z. Bao, *Macromol. Rapid Commun.,* 2016, **37**, 1667-1675.
21 A. Rekondo, R. Martin, A. Ruiz de Luzuriaga, G. Cabañero, H. J. Grande, I. Odriozola, *Mater. Horiz.,* 2014, **1**, 237-240.
22 Y. Chen, A. M. Kushner, G. A. Williams, Z. Guan, *Nat. Chem.,* 2012, **4**, 467-472.
23 X. Yan, Z. Liu, Q. Zhang, J. Lopez, H. Wang, H.-C. Wu, S. Niu, H. Yan, S. Wang, T. Lei, J. Li, D. Qi, P. Huang, J. Huang, Y. Zhang, Y. Wang, G. Li, J. B. H. Tok, X. Chen, Z. Bao, *J. Am. Chem.Soc.,* 2018, **140**, 5280-5289.